Colloids and Surfaces B: Biointerfaces 175 (2019) 428–435

Contents lists available at ScienceDirect

Colloids and Surfaces B: Biointerfaces

journal homepage: www.elsevier.com/locate/colsurfb

Photodegradable coumarin-derived amphiphilic dendrons for DNA binding: Self-assembly and phototriggered disassembly in water and air-water interface

Jia-Yu Ou[a], Yu-Chan Shih[a], Bing-Yen Wang[b,c,d,e,f,g,*], Chih-Chien Chu[a,h,*]

[a] Department of Medical Applied Chemistry, Chung Shan Medical University, Taichung City, Taiwan
[b] Division of Thoracic Surgery, Department of Surgery, Changhua Christian Hospital, Changhua County, Taiwan
[c] School of Medicine, Chung Shan Medical University, Taichung City, Taiwan
[d] Institute of Genomics and Bioinformatics, National Chung Hsing University, Taichung City, Taiwan
[e] School of Medicine, College of Medicine, Kaohsiung Medical University, Kaohsiung City, Taiwan
[f] Ph.D. Program in Translational Medicine, National Chung Hsing University, Taichung City, Taiwan
[g] Center of General Education, Ming Dao University, Changhua County, Taiwan
[h] Department of Medical Education, Chung Shan Medical University Hospital, Taichung City, Taiwan

ARTICLE INFO

Keywords:
Dendrimers
Amphiphilic dendrons
Langmuir analysis
Photocleavage
Gene delivery

ABSTRACT

In this article, we demonstrate the self-assembly and photoresponive behavior of a novel coumarin-based amphiphilic dendron in both aqueous solution and air-water interface. The dendritic structure, namely C-IG_1, was composed of a lipophilic cholesterol and hydrophilic poly(amido amine) (PAMAM) dendron, and the amphiphilic counterpart is interconnected by a photolabile coumarin carbonate ester, enabling the photoinduced degradation of the amphiphiles in protic solvents via S_N1-like mechanism. A Nile red solubilization fluorescence assay suggests a low critical aggregation concentration for the micelle formation of C-IG_1 in aqueous solutions (3.9×10^{-5} M); the Langmuir analysis further indicates that C-IG_1 possesses significant compressibility in air-water interface, eventually forming homogeneous monolayers with a final molecular area (A_0) of 36 Å^2. Notably, the micelles and Langmuir monolayer are quite stable until photo-triggered dissociation based on the photocleavage of C-IG_1 amphiphile activated by 365-nm incident light. Moreover, the transition in interfacial morphology of the Langmuir monolayer during the assembly and photodegradation processes also can be visually analyzed by incorporating Nile red probes with in situ monitoring through fluorescence microscopy. The thin film deposited on a glass substrate by the Langmuir-Blodgett technique also shows a photoresponsive behavior based on the change in the contact angles of a water droplet on the surface upon light stimulation. The binding affinity of C-IG_1 and cyclic DNA determined by the fluorescence quenching analysis of the coumarin reporter suggests a ground-state macromolecular complexation process occurring through polyvalent interactions between the pseudodendrimers and biomacromolecules. The ethidium bromide displacement assay further indicates thus dendriplex formation at low nitrogen-to-phosphorous value (N/P $<$ 1) and confirms that the decomplexation accompanied by DNA release can be achieved through an active phototriggered route under spatiotemporal control.

1. Introduction

Phototriggers provide a useful strategy for the photocontrolled drug delivery system (PDDS) because they enable rapid and accurate spatial and temporal control with external light stimulation [1]. The biological relevant materials containing photocaged building blocks can undergo efficient photolysis through active phototriggers, thereby leading to structural degradation combined with the release of bioactive payloads [2–9]. One of the most well-known light-absorbing photocages is the coumarin family, which enables one- or two-photon–regulated drug release [1,10–13]. Because coumarin derivatives undergo photosolvolysis through a photo S_N1 mechanism, the microenvironment for achieving effective bond cleavage requires access to a nucleophile in a protic media (typically water) [14]. Furthermore, the intrinsic

* Corresponding authors at: Department of Medical Applied Chemistry, Chung Shan Medical University, No. 110, Sec. 1, Jianguo N. Rd., Taichung 40201, Taiwan (C.-C. Chu); Division of Thoracic Surgery, Department of Surgery, Changhua Christian Hospital, No. 135, Nanxiao St., Changhua City 500, Taiwan
E-mail addresses: 156283@cch.org.tw (B.-Y. Wang), jrchu@csmu.edu.tw (C.-C. Chu).

https://doi.org/10.1016/j.colsurfb.2018.12.018
Received 6 August 2018; Received in revised form 28 November 2018; Accepted 8 December 2018
Available online 11 December 2018
0927-7765/

fluorescent nature of the coumarin ring makes these photocages robust fluorescent probes for simultaneously imaging the biodistribution of the PDDS in living tissues [11].

The use of amphiphilic dendron architectures, in which hydrophobic groups at the focal point form pseudodendrimers through a self-assembly process, has facilitated a new type of dendrimer-mediated delivery *in vitro* and *in vivo* [15–22]. Notably, this supramolecular strategy, which enables combining the characteristics of polymers and lipids, can give lead to a synergistic effect, particularly during nucleic acid delivery [23]. Principally, when used as gene vectors, pseudodendrimers apply dynamic and responsive association and dissociation toward nucleic acids [24]. Moreover, complete dendron degradation may be required for effective decomplexation to release nucleic acids. However, experimental and computer-aided simulation data have revealed that the structural degradation of dendrons when bound to nucleic acids becomes ineffective on the transfection timescale, even at lower pH associated with endosomes [25]. This key problem makes gene delivery a challenging task, particularly for the *in vivo* system.

In this study, we developed amphiphilic dendritic scaffolds with photocages for creating a photoresponsive pseudodendrimer that can achieve controlled release under an active light trigger [15]. The amphiphilic structure composed of a hydrophilic poly(amido amine) (PAMAM) dendron and lipophilic cholesterol molecule combines the advantageous gene delivery features of both lipids and polymer vectors. As shown in Fig. 1a, the amphiphilic counterpart is further interconnected by a photolabile coumarin carbonate ester, enabling the photoinduced degradation of the amphiphilic structure (C-IG_1). The arrow indicates an electrophilic allylic carbon, and the C–O bond can be readily cleaved in the presence of weak nucleophiles under light illumination [26]. Consequently, this strategy provides an active route for accelerating nucleic acid release and enhancing gene transfection efficiency. Moreover, to understand the self-assembly process of the amphiphiles and their photoresponsive behavior, the Langmuir technique was introduced for investigating the interfacial phenomenon at the air–water interface [27–29]. We believe that the thus-formed Langmuir monolayers are more fluid and therefore provide a more realistic model for studying DNA binding and phototriggered release.

2. Results and discussion

As shown in Fig. 1b, the azide-functionalized cholesterol and coumarin conjugate ***1*** were synthesized from a commercially available 7-hydroxy-4-methylcoumarin in four steps. On the basis of our design, the cholesterol not only acts as the lipophilic head but also assists cellular uptake by enhancing penetration across a cell membrane. The interconnecting coumarin-derived carbonate ester is highly sensitive to ultraviolet (UV) light, and the photolabile C–O bond (marked in bold) is readily cleaved to recover compound ***2*** and release a free cholesterol molecule. Copper(I)-catalyzed azide-alkyne cycloaddition (CuAAC) between the alkyl-functionalized PAMAM dendrons and ***1*** affords the amphiphilic dendrons, namely C-IG_1 (Fig. 1) [18]. Notably, compared with the conventional PAMAM dendron, this dendritic analogue has two additional primary amine terminals but possesses an inverse tertiary amine branch and amide linkage [30]. Here, the amphiphilic dendron was well-characterized through nuclear magnetic resonance (NMR) and mass spectrometry (MS) analysis. The click conjugation was confirmed according to the appearance of triazole proton resonance, and the observed mass values were consistent with the calculated values of the protonated adducts of C-IG_1.

The time-dependent photolytic reaction of ***1*** was monitored by UV–Vis absorption and fluorescence spectra. The maximum absorption and emission wavelengths of ***1*** were found to be 320 and 390 nm, respectively. As shown in Fig. 2a, the absorbance at 320 nm decreases slightly as the sample solution is exposed to a 365-nm light emitting diode (LED); however, the fluorescence intensity at 390 nm gradually increases with the irradiation time (Fig. 2b). The fluorescence enhancement is evidently attributable to the S_N1-like photolytic reaction of the coumarin ester with an increasing fluorescence quantum yield [14]. Moreover, high-performance liquid chromatography (HPLC) analysis showed the depletion of the retention peak of ***1*** after light exposure (Fig. 2c). Gas chromatography (GC)–MS analysis further confirmed the released cholesterol through photocleavage as the characteristic elution peak (Fig. 2d). All results suggested a successful photoinduced structural degradation of the coumarin derivative.

Because of the amphiphilic structure being composed of a

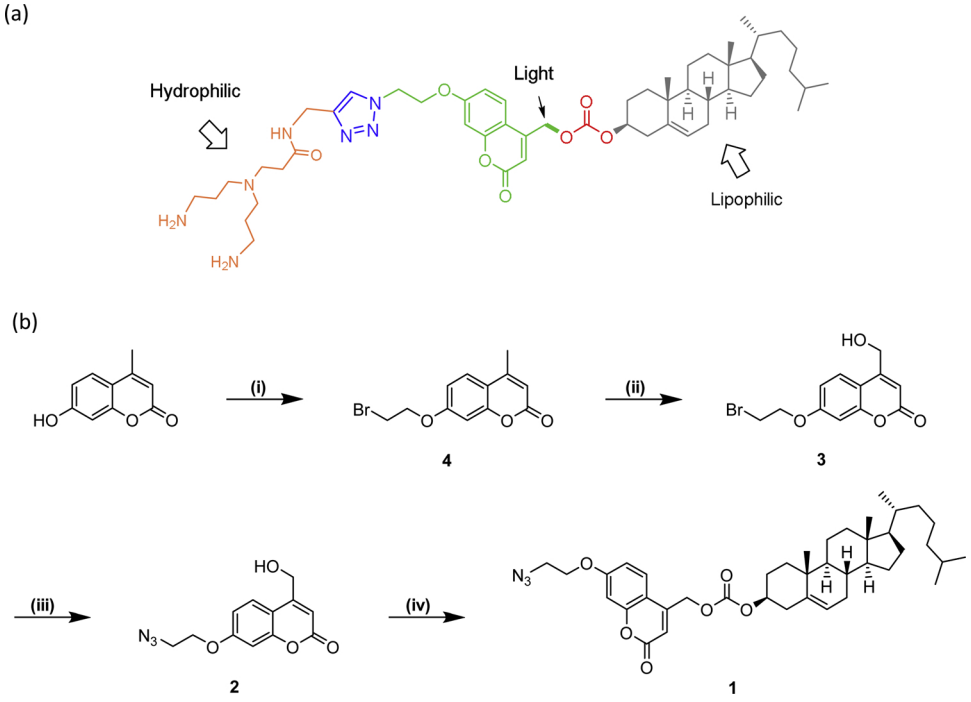

Fig. 1. (a) Chemical structure of a coumarin-based amphiphilic dendron C-IG_1. (b) Synthetic condition for compound ***1***: (i) 1,2-dibromoethane, K_2CO_3, 18-crown-6, THF, 40 °C; (ii) 1. SeO_2, dry toluene, reflux and 2. $NaBH_4$, MeOH, 0 °C to room temperature; (iii) NaN_3, DMF, 50 °C; (iv) cholesteryl chloroformate, pyridine, THF, 50 °C.

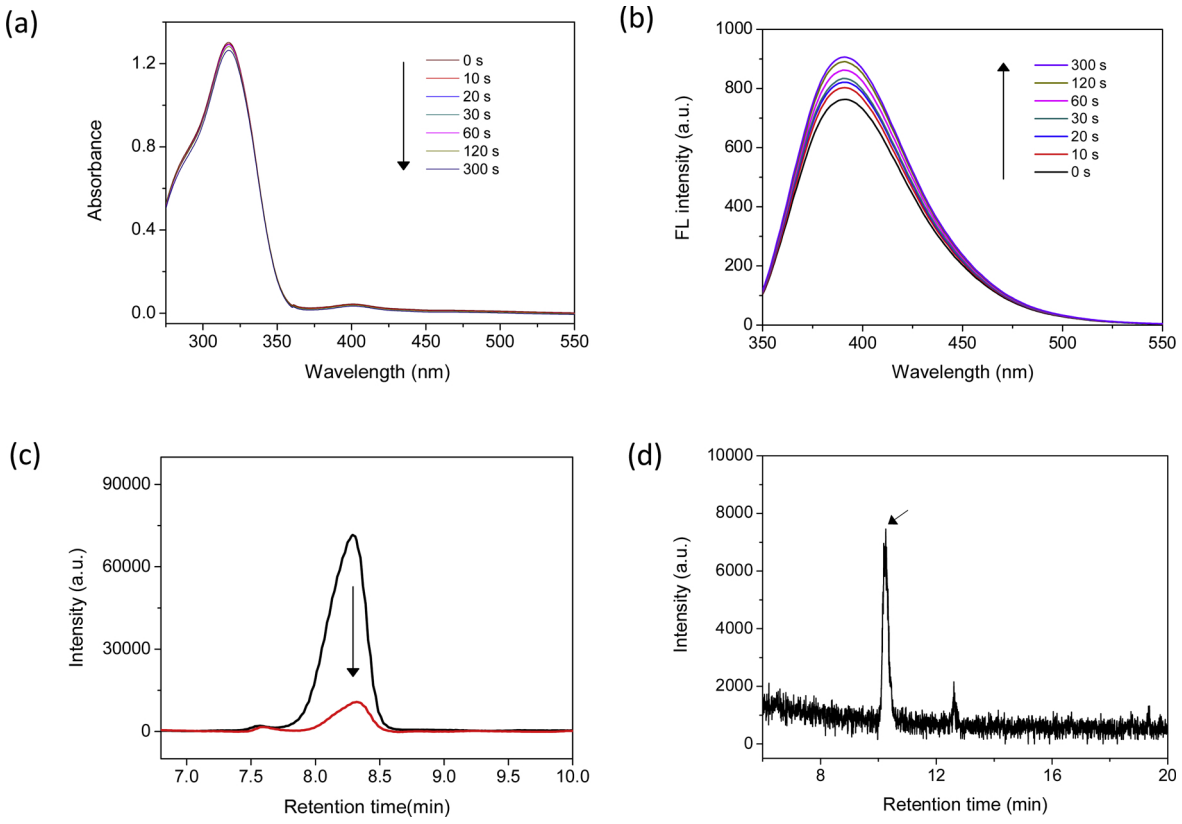

Fig. 2. (a) UV–vis absorption and (b) fluorescence spectra of compound ***1*** recorded upon 365-nm light irradiation at fixed time intervals. (c) HPLC analysis shows the decrease in the retention peak of ***1*** and (d) GC analysis shows the retention peak of free cholesterol released from ***1*** after light excitation.

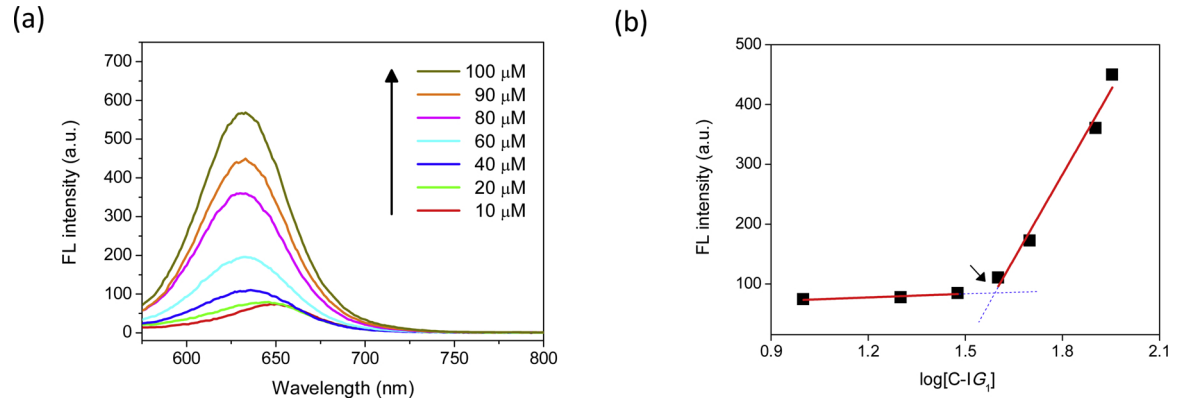

Fig. 3. The Nile red solubilization fluorescence assay for amphiphilic dendron C-IG_1. (a) Fluorescence intensity for the Nile-red probe (2.5 μM) gradually increases as the concentration of dendron increases. (b) The critical aggregation concentration (CAC) was extracted from the intersection of two linear regressions based on lower and higher concentration of dendrons against the fluorescence intensity at 635 nm.

hydrophilic PAMAM dendron and a lipophilic cholesterol, C-IG_1 could self-assemble into Percec-type pseudodendrimers with micelle-like structures in an aqueous medium [31]. This self-assembly process was confirmed using a Nile red solubilization fluorescence assay to detect the formation of a hydrophobic domain of cholesterol within an assembled nanostructure [32]. In this assay, the hydrophobic stain Nile red was gradually solubilized in the micelles and emitted red fluorescence as the concentration of C-IG_1 increases (Fig. 3a). Fig. 3b shows self-assembly with discontinuity in the fluorescence intensity of Nile red at 635 nm, plotted against the increasing dendron concentration at the critical aggregation concentration (CAC). The CAC for C-IG_1 was approximately 39 μM, much lower than that for a coumarin-derived surfactant [33]. Moreover, dynamic light scattering analysis shows that the particle size distribution for C-IG_1 at 100 μM above the CAC value was 117.5 ± 21.4 nm, confirming the amphiphilic dendrons possess effective self-assembly process.

To understand the self-assembly behavior of the amphiphile, the Langmuir technique was introduced to investigate the interfacial phenomenon at the air–water interface. As shown in Fig. 4a, π-A isotherms have three distinguishable phase transitions from a gas (i)-like state to liquid (ii)- and finally solid (iii)-like states, suggesting that C-IG_1 possesses significant compressibility, eventually forming homogeneous Langmuir monolayers upon compression, until the surface pressure of collapse is approximately 50 mN/m. This result evidently suggests that the amphiphilic structure also favors the molecular assembly at the air–water interface. The final molecular area (A_0) in a compressed film determined by extrapolation to zero surface pressure is approximately 36 Å^2 for C-IG_1, consistent with the A_0 of the amphiphilic dendrons with

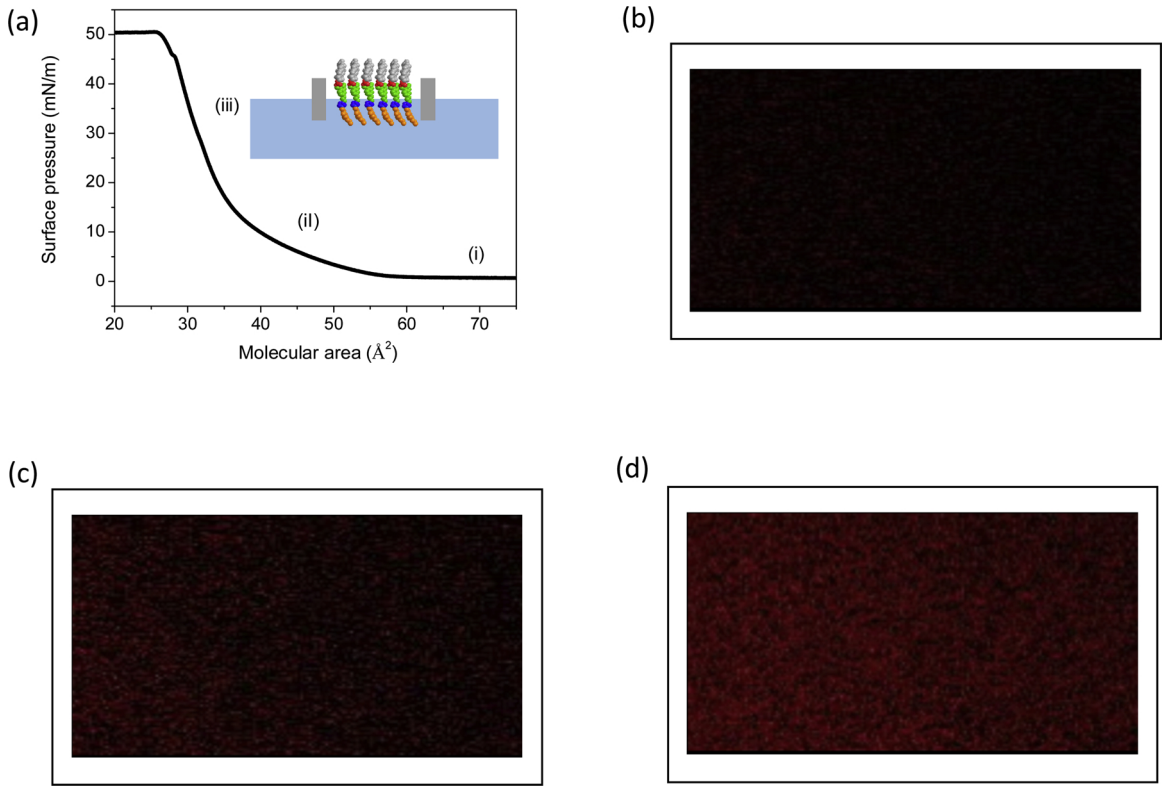

Fig. 4. (a) The Langmuir π-A isotherm for amphiphilic dendron C-IG_1 monolayer at air-water interface with subphase of pure water. Fluorescence micrographs of the Langmuir monolayers doped with the Nile red probes at various surface pressure: (a) 0, (b) 5, and (c) 40 mN/m.

small dendritic branches [28]. Moreover, the interfacial morphology of the Langmuir film under increasing surface pressures was analyzed by incorporating Nile red probes with in situ monitoring through fluorescence microscopy [29]. Fig. 4b–d denotes the fluorescence distributions of the probe molecules under different molecular packings of the amphiphiles in the three states. Fig. 4d illustrates the closely packed and highly fluorescent domains under the surface pressure of 40 mN/m, suggesting the successful formation of a condensed Langmuir monolayer at the interface. This result corroborates with that of the solubilization assay analysis that the emission intensity considerably increases in the presence of the micelle-like assembled structure of the amphiphiles in water. This result also confirms that the C-IG_1 possesses a strong self-assembly capability in both aqueous phases and at the air–water interface.

After confirming that the amphiphilic dendron can process molecular assembly, we examined the photoresponsive behavior of the assembled structures. The photocleavable building block of coumarin ester aids the self-aggregated micelles in readily dissociating under UV irradiation. First, this deformation can be analyzed using micelle-encapsulated Nile red probes. In contrast to the controlled experiment, where the solution stored in darkness only exhibited a slight decrease in fluorescence intensity, 365-nm light irradiation can cause a considerable fluorescence decrement within 5 min, until reaching a plateau (Fig. 5a). This result suggests that the micelles are stable until active light stimulation degrades these self-assembled structures. Second, a Langmuir monolayer at a certain surface pressure (approximately 40 mN/m) and molecular area, maintained by keeping the barriers constant, was prepared. Subsequently, the equilibrium was continuously disturbed through 365-nm light irradiation. Before analysis, control experiment showed that the surface pressure of the monolayer of stearic acids remains constant on light irradiation, suggesting that if the amphiphile is insensitive to UV light, light stimulation does not influence the integrity of the assembled structure. Fig. 5b shows the correlation of elapsed time (t) versus surface pressure, recorded immediately after photostimulation was activated (t = 0). The surface pressure of the monolayer composed of C-IG_1 gradually decreases as the light is turned on (red line); by contrast, this monolayer remains relatively stable in darkness (black line). Notably, the nonlinear decay of the surface pressure following light excitation may be attributable to the first-order kinetics of the S_N1-like photolysis mechanism for coumarin derivatives, because the reaction rate is correlated only with the initial C-IG_1 concentration, and the photoinduced dissociation of C-IG_1 to yield a carbocation intermediate is the rate-determining step for the overall photolytic reaction [14]. In addition, in situ monitoring of the interface morphology by using Nile red probes also indicated that the fluorescence intensity for the assembled pattern decreased on light excitation (Fig. 5c). The visualized images clearly confirm the efficient photodegradation of the Langmuir monolayer.

As shown in Fig. 6, the monolayer at the interface partially collapsed on light exposure because it could be reconstructed through continuous compression in darkness. The surface pressure initially decreased upon light excitation (black arrows) but increased again after barrier compression in darkness. The photoinduced collapse and reconstruction of the monolayer can be alternatively manipulated until the maximum pressure of approximately 50 mN/m is reached. Taken together, in the Langmuir technique, the assembled structure composed of coumarin-based amphiphilic dendrons is consistently highly sensitive to UV light. The bond cleavage between the coumarin ester and cholesterol at the interface results in the collapse of the monolayer under light stimulation. The current Langmuir analysis also confirmed that the photostimulation strategy provides accurate spatial and temporal control over the self-assembled system integrity.

To further reveal the thin-film properties of the amphiphilic C-IG_1, three-layer monolayers were transferred to a glass substrate by using up–down–up strokes based on the Langmuir–Blodgett (LB) technique. Because the coverglass possesses a hydrophilic surface, the bottom layer of the sandwich structure comprises the hydrophilic PAMAM dendron and the upper layer should comprise lipophilic cholesterols (Fig. 7a).

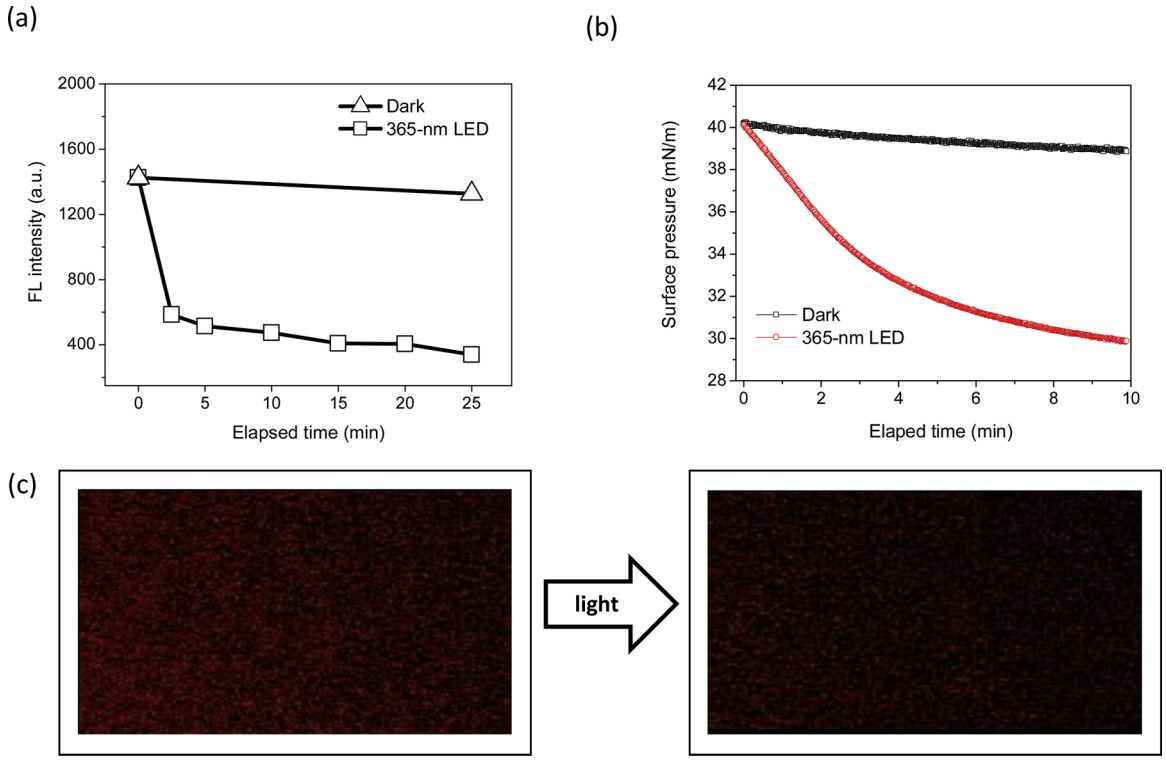

Fig. 5. The change in (a) fluorescence intensity of the Nile-red incorporated micelles ([C-IG_1] = 100 μM) and in (b) surface pressure of the Langmuir monolayer composed of the amphiphilic C-IG_1 upon 365-nm light irradiation at fixed time intervals. (c) Fluorescence micrographs of the Langmuir monolayer (40 mN/m) doped with the Nile-red probes upon light irradiation.

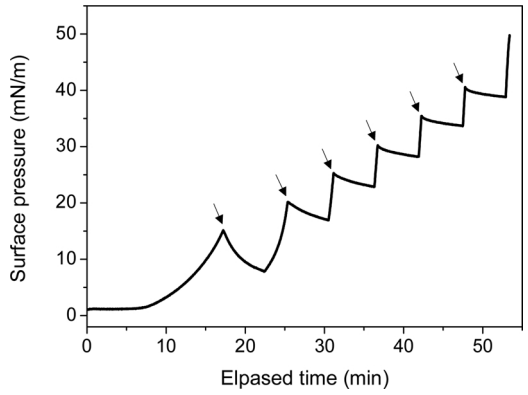

Fig. 6. A stepped control for the collapse and reconstruction of the Langmuir monolayer by alternating photoexcitation and barrier compression processes. The monolayer was first fabricated at 15 mN/m and then repetitively irradiated with 365-nm LED light for 5 min (arrows) and recompressed in dark until designated surface pressure.

From the measurement of static contact angles (Fig. 7b–e), the angle for a water drop on the surface considerably increases from approximately 18° to 90° after three-layer film deposition. This result confirms that the surface becomes a lipophilic domain because of a tidy arrangement of the amphiphiles. Notably, the contact angles gradually decrease when the film is exposed to UV light, implying that the ordering LB film is disturbed by an incident light. The photolabile coumarins undergoing a photolytic reaction cause the structural degradation of the amphiphiles. Accordingly, the LB film of C-IG_1 also exhibits a photoresponsive behavior in a solid state.

After the coumarin-based amphiphilic dendrons self-aggregate into the assembled pseudodendrimers with positively charged peripherals, they can effectively interact with polyanionic bioactive targets, such as DNA, to form dendriplexes through electrostatic interaction. The binding ability of C-IG_1 toward cyclic DNA, a pEGFP-C1 reporter gene (approximately 4700 bp), was first studied through fluorescence titration experiments. In Stern–Volmer analysis, the intrinsic fluorescence of the coumarin moiety enables direct resolution of the binding affinity of the vector and DNA [33]. As shown in Fig. 8, the emission intensity of coumarin at λ = 390 nm gradually decreased with the continuous addition of DNA as the fluorescence quencher, indicating successful binding between the pseudodendrimers and giant DNA through electrostatic association. The Stern–Volmer plot (inset in Fig. 8a) further illustrates a linear correlation between the change in fluorescence intensity and concentration of the quencher, suggesting a static quenching mode for both species. Assuming that the molecular mass for cyclic DNA is approximately 3×10^6 Da, the quenching constant retrieved from the slope is 0.998 μg^{-1}, corresponding to 5.9×10^9 M^{-1}. The value is close to the magnitude of the binding affinity between polymers and proteins rather than that of the groove binding of small molecules (e.g., drug) and DNA [33,34]. Thus, the pseudodendrimer assembled from amphiphilic C-IG_1 is an excellent biomacromolecular binder and the dendriplex formation is a ground-state macromolecular complexation process occurring through polyvalent interactions.

The binding and photoinduced release were analyzed using an ethidium bromide (EtBr) displacement assay [15]. Fig. 8b shows the fluorescence titration experiment by increasing C-IG_1 concentration at constant amounts of DNA and EtBr. Initially, the EtBr undergoes a large increase in fluorescence intensity on intercalation with stacks of nucleic acid base pairs. However, the fluorescence quenching of the EtBr/DNA complexes occurs in the presence of amine-based vectors, engendered by the competitive displacement of EtBr by the vectors. The emission intensity at 590 nm gradually decreases as the nitrogen-to-phosphorus (N/P) ratio increases, suggesting increasing dendriplex formation with increasing C-IG_1 concentration. When the vectors degrade under UV light exposure, DNA should be released and EtBr should reintercalate into the double helix, thus reactivating its fluorescence. Accordingly, Fig. 8c shows the fluorescence increment from the minimum intensity

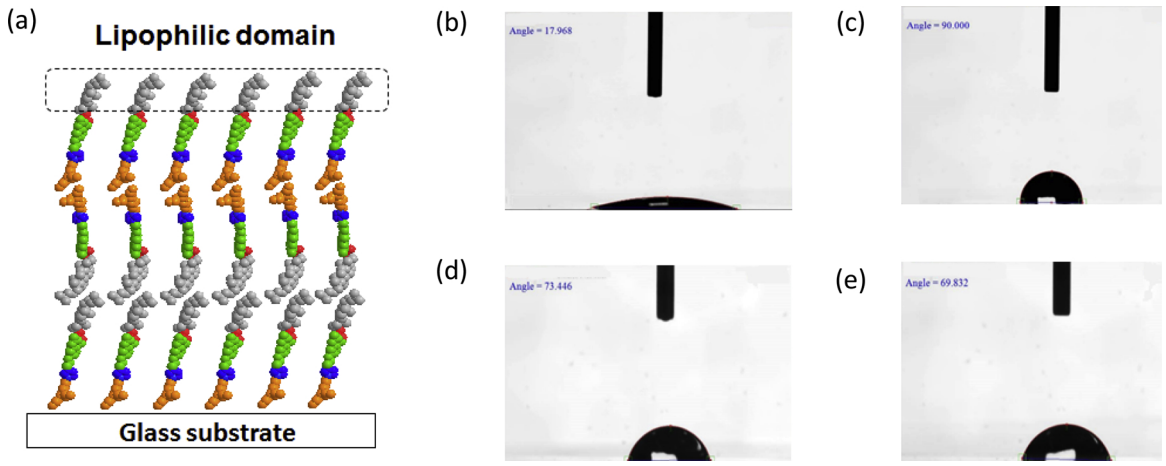

Fig. 7. (a) Three-layer monolayers transferred to a glass substrate by the Langmuir-Blodgett (LB) technique. A contact angle measurement for a water droplet on (b) a clean substrate and (c–e) a LB film-deposited substrate: (c) dark and 365-nm light irradiation for (d) 15 and (e) 30 min.

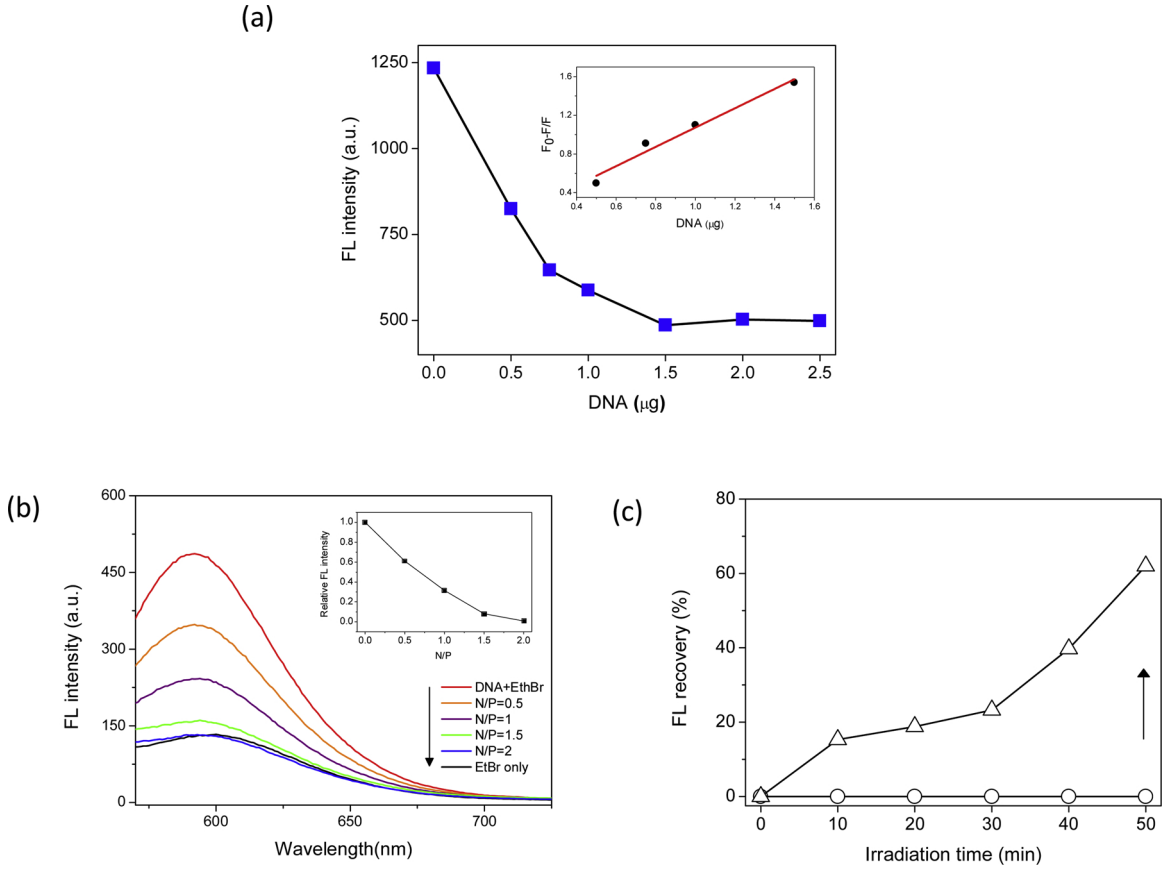

Fig. 8. (a) Fluorescence titration analysis of C-IG_1 (1.5 μM) upon addition of pEGF-C1 (0–2.5 μg). Inset: Stern-Volmer plot for the change in fluorescence intensity at 390 nm as a function of the amount of quencher. (b) Fluorescence titration data of ethidium bromide (EtBr) displacement assay for addition of C-IG_1 to pEGFP-C1 at increasing nitrogen-to-phosphorous (N/P) ratios. The inset shows the correlation of relative fluorescence intensity of EtBr at 590 nm *versus* N/P values. (c) Recovery ratio of the fluorescence intensity for EtBr reintercalating into pEGFP-C1 after dissociation of the C-IG_1/DNA complexes (N/P = 2) upon 365-nm light excitation.

of the DNA/C-IG_1 complexes at N/P ratio = 2 after LED light excitation. By contrast, the fluorescence intensity remained static when the complex solution was maintained in darkness. This result confirms that the photolytic reaction of the vectors induces decomplexation accompanied by DNA release through an active phototriggered route.

After light exposure for 50 min, the fluorescence intensity was partially recovered to approximately 60% of the original magnitude for the emission of the DNA/EtBr complex in the absence of the dendritic vectors (N/P = 0). This result implies that only 60% of DNA is released from the dendriplexes upon light excitation. Thus, the assembled dendrons may be more resistant to the photoinduced disruption than a single dendron is. The Langmuir analysis results also revealed that the assembled structure would soon be recovered under external compression after a partial collapse. Therefore, these electrostatic complexes may be relatively resistant to environmental fluctuation. Although UV light is insufficient to induce complete dissociation of the DNA complexes using a coumarin-derived amphiphilic dendron as the vector, it does assist nucleic acid release.

3. Conclusions

In summary, we successfully synthesized photoresponsive amphiphilic PAMAM dendrons bearing

photolabile coumarin ester building blocks as DNA carriers. The amphiphilic dendrons C-IG_1 exhibit the capability for self-assembly during micelle-like pseudodendrimer formation in an aqueous solution, which was confirmed by spectroscopy and Langmuir isotherm analysis. Based on the bipolar functionality, C-IG_1 also demonstrates substantial binding affinity with cyclic DNA at low N/P ratios. Notably, the thus-formed DNA complexes readily dissociate under UV light irradiation because the coumarin ester group in the dendritic structure undergoes efficient photolytic cleavage, causing effective dendron degradation accompanied by DNA release.

4. Experimental sections

4.1. Materials and instruments

The chemical reagents and organic solvents for materials synthesis were obtained as high-purity reagent-grade from commercial suppliers and used without further purification. Carbamate-protected dendron (Boc-IG_1) was synthesized following the published procedure [15]. ^{1}H (400 MHz) and ^{13}C (75 MHz) NMR spectra were recorded on a Varian Mercury Plus 400 MHz spectrometer at room temperature using $CDCl_3$, DMSO-d_6, methanol-d_4, or D_2O as the solvents. Spectral processing (Fourier transform, peak assignment, and integration) was performed using MestReNova 6.2.1 software. Matrix-assisted laser desorption ionization/time-of-flight (MALDI–TOF) MS was performed on a Bruker AutoFlex III TOF/TOF system in positive ion mode using either 2,5-dihydroxybenzoic acid or α-cyano-4-hydroxycinnamic acid as the desorption matrix. UV–vis absorption spectra was performed on a Thermo Genesys 10S UV–Vis spectrometer. Fluorescence emission spectra was recorded on a Hitachi F-2500 spectrometer. GC–MS was performed on a Hewlett-Packard 5890 series II gas chromatography equipped with 5972 series mass selective detector. HPLC was performed on a JASCO instrument equipped with a MD-2015 PLUS photodiode array detector, covering the wavelengths from 200 to 900 nm with an interval of 1.5 nm. The HPLC analysis was conducted at 25 °C using Dr. Maisch Reprosil 100-Si column (250 × 4.6 mm, normal phase with 5 um porous spherical silica). A solvent mixture of hexane (97%) and isopropanol (3%) was used as a mobile phase and the flow rate was maintained at 1.0 cm^3/min. Photolysis of the ester conjugates were carried out by using light-emitting diodes (LED) at 365 nm and an output power of 10-watt.

4.2. Synthesis of compound 1

To an anhydrous tetrahydrofuran (THF) solution of 7-hydroxy-4-methylcoumarin (528 mg, 1 mmol), K_2CO_3 (1.46 g, 3.5 mmol), and 18-crown-6 (4.36 g, 5.5 mmol), 1,2-diboromoethane (5.69 g, 10 mmol) was added dropwise under N_2. After stirred at 40 °C for 2 days, the volatile was removed by rotatory evaporation, and then the mixture was extracted with CH_2Cl_2 and brine. Combed organic phase was dried over anhydrous magnesium sulfate, and rotatory evaporation to dryness afforded crude product. Flash column chromatography (SiO_2) yields compound **4** (76%, R_f = 0.55, ethyl acetate/hexane = 1:1).

A mixture of **4** (609 mg, 2.2 mmol) and SeO_2 (715 mg, 6.6 mmol) dissolved in anhydrous toluene was heated under reflux for 2 days, and then the volatile was removed by rotatory evaporation. The mixture dissolved in anhydrous methanol was added dropwise into a methanol solution of $NaBH_4$ (83.9 mg, 0.28 mmol) under ice bath, and the reaction was further stirred at room temperature for 1 day. The reaction was quenched by dilute HCl solution and extracted with ethyl acetate. Flash column chromatography (SiO_2) yields compound **3** (21%, R_f = 0.28, ethyl acetate/hexane = 1:1).

A dimethylformamide solution of **3** (83.9 mg, 0.28 mmol) and NaN_3 (20.1 mg, 0.3 mmol) was stirred at 50 °C for 1 h under N_2. The solvent was removed under vacuum, and the mixture was extracted by ethyl acetate/brine. Combined organic phase was dried over magnesium sulfate, and rotatory evaporation to dryness afforded compound **2** (97%, R_f = 0.25, ethyl acetate/hexane = 1:1). A THF solution of **2** (100 mg, 0.38 mmol), cholesteryl chloroformate (249 mg, 1.4 mmol), and pyridine (75 μL, 0.93 mmol) was stirred at 50 °C for overnight under N_2. The solvent was removed under vacuum, and the crude product was purified by flash column chromatography (SiO_2) to give compound **1** (76%, R_f = 0.8, ethyl acetate/hexane = 1:1). The overall yield for the four-step reaction is 12%, and this lower yield is mainly attributed to the heterogeneous allylic oxidation of compound **4** and SeO_2. ^{1}H-NMR (400 MHz, $CDCl_3$) for ***1***: δ = 7.44 (d, J = 8.8 Hz, 1 H), 6.91 (dd, J = 8.8, 2.5 Hz, 1 H), 6.86 (d, J = 2.5 Hz, 1 H), 6.40 (t, J = 1.4 Hz, 1 H), 5.41 (d, J = 5.1 Hz, 1 H), 5.30 (d, J = 1.4 Hz, 2 H), 4.50–4.58 (m, 1 H), 4.21 (t, J = 5.1 Hz, 2 H), 3.67 (t, J = 5.1 Hz, 2 H), 2.43 (m, 2 H), 2.06 – 0.82 (m, 38 H), 0.68 (s, 3 H); ^{13}C-NMR (75 MHz, $CDCl_3$): δ = 161.6, 160.8, 155.6, 154.1, 148.9, 139.3, 124.9, 123.5, 113.2, 111.2, 110.8, 102.0, 79.3, 67.7, 64.3, 56.9, 56.3, 50.1, 42.5, 39.9, 39.7, 38.2, 37.0, 36.8, 36.4, 36.01, 32.1, 32.0, 28.5, 28.3, 27.9, 24.5, 24.0, 23.1, 22.8, 21.3, 19.5, 18.9, 12.1.

4.3. Synthesis of the click cluster C-IG$_1$

An anhydrous CH_2Cl_2 solution of compound **1** (87.7 mg, 0.13 mmol), Boc-protected IG_1 (76.2 mg, 0.16 mmol), and CuBr (22.8 mg, 0.16 mmol) was vigorously stirred at room temperature until the complete disappearance of compound **1**. The resulting solution was then extracted with CH_2Cl_2; the organic phase was washed with aqueous ammonia solution to remove copper catalyst and then dried over magnesium sulfate. Rotatory evaporating to dryness yields the Boc-protected click clusters C-IG_1 without further purification (96%). Boc-deprotection is readily carried out by acid-promoted hydrolysis. Trifluoroacetic acid (0.14 mL, 1.9 mmol) was added dropwise into an anhydrous CH_2Cl_2 solution of Boc-protected C-IG_1 (51.6 mg, 45 μmol). The mixture was then stirred under room temperature for 3 days, and the volatiles were removed under reduced pressure. The mixture was rinsed with hexane repetitively to remove excess acid, and then freeze-drying afforded amphiphilic dendron C-IG_1 as yellowish fluffy powders (97%). For Boc-protected C-IG_1, ^{1}H-NMR (400 MHz, $CDCl_3$): δ = 8.20 (bs, 1 H), 7.78 (s, 1 H), 7.43 (d, 1 H), 6.86 (d, 1 H), 6.81 (s, 1 H), 6.40 (s, 1 H), 5.42 (m, 1 H), 5.29 (s, 2 H), 5.01 (bs, 2 H), 4.79 (t, 2 H), 4.54–4.58 (m, 1 H), 4.51 (d, 2 H), 4.43 (t, 2 H), 3.05–3.10 (m, 4 H), 2.64 (t, 2 H), 2.38–2.44 (m, 7 H), 2.32 (t, 2 H), 0.85–2.04 (m, 60 H), 0.68 (s, 3 H). For C-IG_1, ^{1}H-NMR (400 MHz, CD_3OD): δ = 8.17 (s, 1 H), 7.60 (d, 1 H), 6.98 (d, 1 H), 6.91 (s, 1 H), 6.28 (s, 1 H), 5.42 (s, 1 H), 5.37 (s, 2 H), 4.39–4.57 (m, 5 H), 3.52 (s, 2 H), 3.06 (s, 6 H), 2.80 (s, 2 H), 2.41 (s, 2 H), 2.15 (s, 4 H), 0.86–2.07 (m, 38 H), 0.70 (s, 3 H); MALDI-TOF-MS: Cacld. For $(M+H)^+$ $C_{52}H_{80}N_7O_7$: 914.61 Da; Found: 914.28 Da.

4.4. Nile-red solubilization assay

Nile red stock solution (2.5 mM) was prepared in ethanol, and a dendron stock solution was prepared in PBS buffer at various concentrations depending on the starting concentration for the assay. Aliquots of the stock solution were taken and diluted with PBS to the desired concentration in a 1 mL assay volume. Nile red (1 μL) was added and the fluorescence emission was measured on a spectrofluorometer using an excitation wavelength of 550 nm. Fluorescence intensity was recorded at 635 nm. The photolytic reaction for the single molecule and the micelles in the solutions was performed by irradiating the sample solutions prepared in a quartz cuvette (1 cm x 1 cm) under a 365-nm LED. The distance between the sample and light source was kept at approximately 3 cm, and then the exposed solutions were analyzed by UV–vis and fluorescence spectroscopy.

4.5. Preparation of the Langmuir monolayers

A computer-controlled Langmuir trough (364 mm x 75 mm, KN2002 KSVNIMA) equipped with a Wilhelmy plate for surface pressure measurement was used obtain the surface pressure-area per molecule (π-A) isotherms. A monolayer at the air/water interface in the trough can be symmetrically compressed with two Teflon barriers at a given rate. Before each run, the trough was first filled with Millipore (18.2 MΩ cm) water as the subphase, and the surface pressure of the air/water interface was then zeroed. A chloroform solution of the compounds was then spread at the interface, and a period was allowed for solvent evaporation and for the system equilibrium. The monolayer was continuously compressed at a rate of 5 mm^2/min to record π-A isotherms with in situ fluorescence microscope observation (Axioskop, Carl Zeiss). The Nile red dye was selected the fluorescence probe for monitoring the assembly process at the interface. The excitation/emission wavelengths were selected by an appropriate beam splitter/filter combination for the probes, and the monolayer was observed by using 50-fold magnification of an objective lens. For the photolytic reaction occurred at the air/water interface, the monolayer formed at a certain surface pressure and molecular area, maintained by keeping the barriers constant, was exposed to 365-nm LED irradiation. The change of the surface pressure with irradiation time was then recorded.

4.6. Contact angle measurement for the Langmuir-Boldgett films

The monolayer at surface pressure of 40 mN/m was transferred to a cover glass (2 cm x 2 cm) through a Langmuir-Blodgett (LB) deposition technique in a vertical dipping trough. The glass substrate was pre-rinsed with a piranha solution to yield a clean hydrophilic surface, and the LB film was fabricated by repetitive “up-down-up” strokes with a speed of 2 mm/min to form a sandwich structure composed of three molecular layers of the amphiphilic dendorn. The static contact angle for a water drop on thus-prepared LB film was then measured by a contact angle meter (CAM120, Creating Nano Technologies).

4.7. Fluorescence titration experiment

The titration experiments were carried out by fixing the concentration of fluorescence indicator C-IG_1 (1.5×10^{-9} mol) and varying the addition amount of DNA. The excitation and emission wavelengths was 320 nm and 390 nm, respectively, based on the intrinsic fluorescence feature for the coumarin moiety. The Stern-Volmer equation is utilized for the fluorescence quenching data process:

Where F_0 and F are the emission intensities in the absence and presence of quencher, K is a static quenching constant, and [Q] is the concentration of DNA.

4.8. EtBr displacement assay

0.5 mL of pEGFP-C1 solution (1 μg/mL) and 7 μL of EtBr solution (0.1 mg/mL) were mixed thoroughly in PBS buffer, followed by adding 8 μL of the dendron solutions to the desired N/P values. EtBr in ultrapure water was measured as the background fluorescence of EtBr, and the solution that only contains pEGFP-C1 and EtBr in 1:1 binding ratio corresponds to the N/P = 0 with maximum emission intensity. The fluorescence emission was measured on a spectrofluorometer using an excitation of 540 nm, and the emission spectra were recorded from 540 nm to 700 nm.

Acknowledgments

The authors would like to thank Changhua Christian Hospital (105-CCH-IST-124), Chung Shan Medical University, and Ministry of Science and Technology (MOST-105-2119-M-040-001) of Taiwan for financially supporting this research. The authors also grateful to Prof. Chien-Hsiang Chang at National Cheng Kung University (Taiwan) for support with fluorescence microscopy analysis on the Langmuir films.

References

[1] J. Olejniczak, C.-J. Carling, A. Almutairi, J. Controlled Release 219 (2015) 18–30.
[2] S.O. Poelma, S.S. Oh, S. Helmy, A.S. Knight, G.L. Burnett, H.T. Soh, C.J. Hawker, J. Read de Alaniz, Chem. Commun. 52 (2016) 10525–10528.
[3] P. Thapa, M. Li, M. Bio, P. Rajaputra, G. Nkepang, Y. Sun, S. Woo, Y. You, J. Med. Chem. 59 (2016) 3204–3214.
[4] J.S. Basuki, F. Qie, X. Mulet, R. Suryadinata, A.V. Vashi, Y.Y. Peng, L. Li, X. Hao, T. Tan, T.C. Hughes, Angew. Chem. 129 (2017) 986–991.
[5] M. Bio, P. Rajaputra, I. Lim, P. Thapa, B. Tienabeso, R.E. Hurst, Y. You, Chem. Commun. 53 (2017) 1884–1887.
[6] M. Karimi, P. Sahandi Zangabad, S. Baghaee-Ravari, M. Ghazadeh, H. Mirshekari, M.R. Hamblin, J. Am. Chem. Soc. 139 (2017) 4584–4610.
[7] R.R. Nani, A.P. Gorka, T. Nagaya, T. Yamamoto, J. Ivanic, H. Kobayashi, M.J. Schnermann, ACS Cent. Sci. 3 (2017) 329–337.
[8] Y. Yang, J. Mu, B. Xing, Photoactivated drug delivery and bioimaging, Wiley Interdiscip. Rev.: Nanomed. Nanobiotechnol. 9 (2017) e1408.
[9] E.D. Anderson, A.P. Gorka, M.J. Schnermann, Nat. Commun. 7 (2016) 13378.
[10] M. Gangopadhyay, S.K. Mukhopadhyay, S. Karthik, S. Barman, N.D. Pradeep Singh, MedChemComm 6 (2015) 769–777.
[11] S. Barman, S.K. Mukhopadhyay, M. Gangopadhyay, S. Biswas, S. Dey, N.D.P. Singh, J. Mater. Chem. B 3 (2015) 3490–3497.
[12] T. Furuta, S.S.H. Wang, J.L. Dantzker, T.M. Dore, W.J. Bybee, E.M. Callaway, W. Denk, R.Y. Tsien, Proc. Natl. Acad. Sci. U. S. A. 96 (1999) 1193–1200.
[13] Q. Lin, C. Bao, G. Fan, S. Cheng, H. Liu, Z. Liu, L. Zhu, J. Mater. Chem. 22 (2012) 6680–6688.
[14] T. Eckardt, V. Hagen, B. Schade, R. Schmidt, C. Schweitzer, J. Bendig, J. Org. Chem. 67 (2002) 703–710.
[15] Y.-S. Lai, C.-L. Kao, Y.-P. Chen, C.-C. Fang, C.-C. Hu, C.-C. Chu, New J. Chem. 40 (2016) 2601–2608.
[16] B.N.S. Thota, Hv. Berlepsch, C. Bottcher, R. Haag, Chem. Commun. 51 (2015) 8648–8651.
[17] X. Liu, C. Liu, J. Zhou, C. Chen, F. Qu, J.J. Rossi, P. Rocchi, L. Peng, Nanoscale 7 (2015) 3867–3875.
[18] C.-H. Hung, W.-W. Chang, S.-C. Liu, S.-J. Wu, C.-C. Chu, Y.-J. Tsai, T. Imae, J. Biomed. Mater. Res. A 103 (2015) 1595–1604.
[19] T. Yu, X. Liu, A.-L. Bolcato-Bellemin, Y. Wang, C. Liu, P. Erbacher, F. Qu, P. Rocchi, J.-P. Behr, L. Peng, Angew. Chem. Int. Ed. 51 (2012) 8478–8484.
[20] Y. Cao, X. Liu, L. Peng, Front. Chem. Sci. Eng. (2017) 1–13.
[21] C. Chen, P. Posocco, X. Liu, Q. Cheng, E. Laurini, J. Zhou, C. Liu, Y. Wang, J. Tang, V.D. Col, T. Yu, S. Giorgio, M. Fermeglia, F. Qu, Z. Liang, J.J. Rossi, M. Liu, P. Rocchi, S. Pricl, L. Peng, Small 12 (2016) 3667–3676.
[22] S.P. Jones, N.P. Gabrielson, C.-H. Wong, H.-F. Chow, D.W. Pack, P. Posocco, M. Fermeglia, S. Pricl, D.K. Smith, Mol. Pharm. 8 (2011) 416–429.
[23] D.J. Welsh, D.K. Smith, Org. Biomol. Chem. 9 (2011) 4795–4801.
[24] A. Barnard, D.K. Smith, Angew. Chem. Int. Ed. 51 (2012) 6572–6581.
[25] A. Barnard, P. Posocco, S. Pricl, M. Calderon, R. Haag, M.E. Hwang, V.W.T. Shum, D.W. Pack, D.K. Smith, J. Am. Chem. Soc. 133 (2011) 20288–20300.
[26] Q. Lin, Q. Huang, C. Li, C. Bao, Z. Liu, F. Li, L. Zhu, J. Am. Chem. Soc. 132 (2010) 10645–10647.
[27] J. Lee, C.-H. Chang, Soft Matter 10 (2014) 1831–1839.
[28] M. Guillot-Nieckowski, D. Joester, M. Stöhr, M. Losson, M. Adrian, B. Wagner, M. Kansy, H. Heinzelmann, R. Pugin, F. Diederich, J.-L. Gallani, Langmuir 23 (2007) 737–746.
[29] H. Nakahara, S. Lee, G. Sugihara, C.-H. Chang, O. Shibata, Langmuir 24 (2008) 3370–3379.
[30] A.Y.-T. Huang, C.-H. Tsai, H.-Y. Chen, H.-T. Chen, C.-Y. Lu, Y.-T. Lin, C.-L. Kao, Chem. Commun. 49 (2013) 5784–5786.
[31] D.A. Tomalia, New J. Chem. 36 (2012) 264–281.
[32] P. Greenspan, E.P. Mayer, S.D. Fowler, J. Cell Biol. 100 (1985) 965–973.
[33] X. Yang, X. Jian, J. Wang, H. Zhang, F. Jiang, Colloids Surf. Physicochem. Eng. Aspects 462 (2014) 170–178.
[34] J.S. Mandeville, H.A. Tajmir-Riahi, Biomacromolecules 11 (2010) 465–472.